Communication

Atomic Distance Tuning Effect for Nucleation in Liquid Iron

M. XU, X. GE, W. YAO, S. TANG, W. LU, M. QIAN, Y. FU, H. XIE, T. XIAO, Q. HU, J. LI, and M. XIA

Liquid structural evolution of iron with various oxides was tracked from above liquidus to undercooling temperatures using an *in situ* high-energy X-ray diffraction method. The icosahedral-like orders and its enhancement with the decreasing temperature in all the liquids investigated suggest that icosahedral-like orders are not the sole reasons responsible for the variation of undercooling. The reduction of nearest-neighbor distance (r_1) tuned by catalyzers contributes to the enhanced nucleation behavior of liquid iron.

https://doi.org/10.1007/s11661-018-4807-9

Turnbull[1] proposed that nucleation behavior of crystals in an undercooled liquid is related to the catalyzer it contains, which can be estimated by lattice disregistry between the catalyzer and the nucleated solid. However, even under the same thermal and substrate conditions, a nucleation system can exhibit distinct undercooling values.[2–4] This phenomenon suggests that there are unknown factors affecting nucleation process. To comprehend this puzzle, liquid structure was proposed as an important clue responsible for the variations observed in undercooling.[5,6] Frank[7] hypothesized a theory to explain the origin of undercooling by assuming liquid is composed of icosahedral short-range orders (ISROs). The proposed ISRO has six fivefold symmetry axes,[7] which is incompatible with the crystal translational periodicity. This structural dissimilarity is regarded as the atomic structural origin of the detected undercooling (nucleation energy barrier).

Many experimental and simulation evidences have verified the Frank's hypothesis, where ISRO was identified in metallic liquids, especially in liquid iron.[8–10] The ISRO can be a perfect or distorted fivefold symmetry structure,[11] both can decrease the barrier to nucleation of the metastable i-phase[12] or metallic glass.[13] More recently, the concept of ISRO was considered as the leading structure for icosahedral quasicrystals (iQC) to act as a template for nucleation of crystalline solids, *e.g.*, face-centered-cubic (fcc)-Al in Al-Zn-Cr alloys.[14] Thus, the obtained results suggest that ISRO might be a key intermediate structure for crystal nucleation, i-phase formation, and glass transition during liquid-to-solid transition process.

The earlier study on the effect of the substrate on atomic ordering in liquid was observed through high-resolution transmission electron microscopy (HRTEM) by Howe[15] and Oh *et al.*[16] Layer ordering and in-plane ordering were identified simultaneously in the first few layers adjacent to the liquid/substrate interface.[15–18] Greer[19] pointed out that such ordering could affect the nucleation either positively or negatively, depending on substrate template effect. State-of-art experimental studies[20–23] have shown that indeed the substrate can affect the nucleation behavior of new crystals but the ordering effect on the liquid is missed in these studies. For instance, there is little information about how the liquid ordering takes part in the nucleation process and how the ordering itself is affected by the substrate. In these researches, Schülli *et al.*[20] investigated the substrate template's effects of three different Si substrates on the undercooling of AuSi droplets, but the real reconstruction process of liquid atoms was not observed. Reichert *et al.*[21] pointed out that the substrate was able to capture liquid clusters in preferred orientations, giving rise to orientational alignment of new crystals during nucleation. The other evidences can be referred to the nucleation of Al[22] and Al-Cu[23] on various substrates but there is no discussion of the role of the substrate on liquid structure as well.

In this paper, we focus on identifying the atomic structural evolution of liquid iron under the influence of the *in situ*-formed iron oxides during the freezing process. These oxides normally lead to different undercoolings even under the same thermal conditions.[24,25] In order to understand the atomic structural origin of the difference in undercooling, structure factors and pair distribution functions of the liquid are tracked from above the liquidus to the undercooled state. The mechanism behind the difference is discussed based on the atomic structural similarity among the investigated iron liquids, the corresponding substrates and the final iron crystal.

Ingot samples with or without oxides were prepared by arc-melting of high-purity elemental Fe (99.99 pct) in

M. XU, X. GE, W. YAO, S. TANG, W. LU, Q. HU, J. LI, and M. XIA are with the School of Materials Science and Engineering, Shanghai Jiao Tong University, Shanghai 200240, China. Contact e-mail: mingxu.xia@sjtu.edu.cn M. QIAN is with the Centre for Additive Manufacturing, School of Engineering, RMIT University, Melbourne, VIC 3000, Australia. Y. FU, H. XIE, and T. XIAO are with the Shanghai Synchrotron Radiation Facility, Shanghai Institute of Applied Physics, Shanghai 215600.
Manuscript submitted April 19, 2018.
Article published online July 16, 2018

a water-cooled copper hearth under an oxygen-filled atmosphere (400 Pa). The preparation details and oxide identification can be found in Reference 25. The mean spatial diameter and the number density are 3.08 ± 0.43 (μm) and $(5.5 \pm 0.9) \times 10^{13}$ (m^{-3}) for Fe_3O_4, and 3.28 ± 0.49 (μm) and $(4.3 \pm 0.4) \times 10^{13}$ (m^{-3}) for FeO, respectively. The average distances between the oxide particles were 26.3 ± 1.5 μm for Fe_3O_4 particles and 28.5 ± 0.9 μm for FeO particles. Levitated samples with different oxides were then used to investigate liquid structural evolution during cooling procedure. High-energy X-ray diffraction (HE-XRD) measurements were performed at specific collection temperatures on BL13W1 at Shanghai synchrotron radiation facility (SSRF) equipped with a monochromatic beam which had an energy level of 72.095 keV and a wavelength of 0.17199 Å. The diffraction patterns were recorded using a Perkin Elmer Si 1621 detector, and the exposure time for data collection was 6 seconds. The raw 2D data were integrated from X-ray intensity profiles using FIT2D program (ref. Supplementary Data),[26] and transformed to 1D profile. The scattering intensities were corrected for absorption, polarization, coherent scattering, Compton scattering, and multiple scattering contributions. Then, structure factor S(Q) of liquid can be derived from diffraction intensity as a function of Q (ref. Supplementary Data), where Q is the scattering vector magnitude. The measurement was acquired over a range of Q values from 1 to 16 $Å^{-1}$ using a rapid-acquisition pair distribution function technique.

Figure 1 displays the S(Q) and the corresponding enlarged second peaks. For oxide-free pure iron, we chose eight temperatures ranging from 1810 °C, *i.e.*, 272 °C above T_m, to 1380 °C, *i.e.*, 158 °C below T_m for survey experiments in order to capture significant evidence for structural changes in the liquid on nucleation. For oxide-contained liquid iron, two temperatures were selected in both the superheating and undercooling zones for a comparison.

The S(Q) for all liquids oscillated well around unity over the entire range of Q values, reflecting the quality of the experimental data.[27] The primary peak increased in intensity and shifted to the high Q value end with a decrease in temperature, as shown in the insets (Figures 1(a) through (c)). It indicates that the degree of order in the liquid becomes increasingly pronounced, corresponding to the expected increase in density. A shoulder on the right-hand side of the second peak is observed for all measured S(Q) curves of the three different liquids, as clearly seen in Figures 1(d) through (f). Such a feature has been identified as a signature of ISRO from the theoretical study of Sachdev and Nelon[28] and was evidenced in liquid iron elsewhere.[8–10] It should be noticed that this feature becomes more pronounced with the decreasing temperature and also more prominent in the Fe_3O_4-contained liquid as indicated by the enhanced intensity (Figures 1(d) through (f)).

The pair distribution function, g(r), was calculated from Fourier transformation of S(Q) as shown in Figure 2. The nearest-neighbor distances (r_1) can be obtained from the location of the first maximum of g(r), which is approximately 2.550 Å for both pure iron liquid and FeO-contained liquid iron at the given undercooled temperature. Compared with those of pure liquid iron and FeO-contained liquid iron, the value of r_1 for Fe_3O_4-contained liquid iron slightly decreases to about 2.544 Å at the same temperature. The intensity of g(r) increases with the decreasing temperature and is slightly higher in Fe_3O_4-contained liquid as displayed in the insets of Figure 2. The same temperature effect on atomic g(r) were also found in Al, Cu, and Cu-Zr melts[29] which suggests that the variation of g(r) with temperature is a common phenomenon of liquid metal. The coordination number, $Z = \int_{r^1}^{r^2} 4\pi\rho r^2 g(r)dr$, of the liquid was calculated from the entire area under the first peak by using the first (r^1) and second (r^2) minima as integration boundaries, where ρ denotes the atomic density. From Figure 2, the r^1 and r^2 have similar values in all three liquids, which lead to an approximate $Z = 12$. The observed values ($Z \sim 12$) at $\sim T_m$ and the shoulder on the second peak of S(Q) are compatible with a few types of SRO including icosahedral-like, fcc-like or hexagonal close packing-like (hcp). However, further evaluation by simulation[28] suggested that the SRO tends to be icosahedral-like orders in liquid iron.

The atomic structure difference was further verified by plotting r_1 and Z values against liquid temperatures as shown in Figure 3. For the liquid without oxide, the r_1 value shifted from 2.555 ± 0.001 Å at 1810 °C to 2.547 ± 0.000 Å at 1380 °C as shown in Figure 3(a). The r_1 value of FeO-contained liquid iron showed nearly the same trend with that of the pure iron liquid from 2.553 ± 0.001 Å at 1565 °C to 2.549 ± 0.001 Å at 1428 °C. As for the Fe_3O_4-contained liquid iron, the r_1 value also decreased with the decreasing temperature but with a much smaller value from 2.547 ± 0.001 Å at 1580 °C to 2.544 ± 0.001 Å at 1478 °C. In fact, the r_1 value of iron crystal is 2.539 Å at the T_m, which is smaller than those of all three liquids but closer to that of the Fe_3O_4-contained liquid iron. It decreases as temperature drops (2.534 Å at 1400 °C), considering the thermal contraction of the crystal.[30] From the above analysis, we have the following sequence of r_1 at $\sim T_m$, *i.e.*, r_1 (liquid iron) $\approx r_1$ (FeO-contained liquid iron) $> r_1$ (Fe_3O_4-contained liquid iron) $> r_1$(solid iron). However, the Z increases linearly with the decreasing temperature as shown in Figure 3(b). The regression coefficient (R^2) of the best fitting is 0.99, indicating an intimate relationship of Z with temperature regardless of the catalyzer. The trends observed in oxide-contained iron liquids indicate that oxide does not affect the coordination number of the liquid but changes the nearest atomic distance depending on the substrate.

It should be noticed that solute element affects the nucleation efficiency in terms of growth restriction factor Q and the formation of a compound.[31–33] In our study, the samples are taken from the same arc melted ingot, undergoing the same thermal cycle condition. Therefore, the oxygen content in the iron melts contained two different oxide particles are consistent with each other, resulting in a slight difference in liquid structures between them. Apart from solute effect,

substrate particles are also able to tune the nucleation behavior in terms of ordering and undercooling through the substrate template effect as discussed in previous sections.[14–16,18,21] But the information about the effect of substrate on the structure of SRO remains ambiguous. Schneider[34] indicated that Cu segregated to a crystalline Si/liquid Al-alloy interface in terms of nanoscale islands rather than monolayer. Pouget[35] found that the aggregation of prenucleation clusters led to the nucleation of amorphous nanoparticles which assembled at the template and formed calcium carbonate crystals after reaching a critical size. These clusters may disperse in the melt under the role of melt flow, resulting in a reduction of the nearest-neighbor distance (Figure 3(a)).

In Figures 4(a) through (d), we present the deduced XRD pattern and reduced pair distribution function G(r) curves of the catalyzing oxides based on the ordinary X-ray diffraction data with the wave length $\lambda = 1.54$ Å obtained from the standard powder diffraction file [PDF, card numbers 19-0629 for Fe_3O_4 and 06-0615 for FeO], with a view to correlating the atomic structure of the nucleating liquid with the corresponding substrate. The first peak was observed at 1.99 Å for Fe_3O_4 crystal, which is very close to the first nearest distance between iron and oxygen (*i.e.*, the length of Fe-O bond) at room temperature.[36,37] According to the thermal expansion of the crystal,[38] the change in the r_1 value of Fe_3O_4 crystal with the increasing temperature is shown in Figure 3(a). At $T_{m,\,Fe}$ of pure iron, the r_1 value can be extrapolated as 2.168 Å, which is much smaller than those of the liquids and pure iron crystal at the same temperature. Figures 4(c) and (d) give the r_1 value of FeO crystal obtained from the G(r) at room temperature, 2.120 Å and the extrapolated r_1 value for FeO at $T_{m,\,Fe}$, 2.248 Å. The r_1 value is much larger than that of Fe_3O_4 at the same temperature but close to that of iron. Here, we obtain r_1 sequence for two oxides at $T_{m,\,Fe}$ as r_1 (FeO crystal) > r_1 (Fe_3O_4 crystal). Combining the r_1 sequence of the liquids and pure iron crystal, this leads to an assumption that a larger r_1 of substrate (FeO) will lead to a larger r_1 of liquid. Apart from this, the approximate equal r_1 values of liquid iron with and without FeO particles also indicate FeO catalyzer has a weaker effect on liquid structure compared with Fe_3O_4.

In our experiment, a denser atomic distance was obtained in Fe_3O_4-contained iron liquid with the smallest substrate r_1, while the larger r_1 of FeO leads to a less dense atomic distance in the liquid. This finding indicates that the liquid system is more likely to be a tension system. The denser substrate will attract the atoms in liquid toward a closer atomic distance and a similar Z but may not be close enough to the same as the substrate, as indicated in Figure 3(a). The nucleation energy barrier depends on the atomic distance difference between SRO structure of the liquid and the corresponding crystal structure, given a similar atomic structural type (an identical Z value). If the atomic distance of SRO is close to the crystal structure, the required nucleation energy is thus much lower than those liquid with a larger atomic distance. In this study, the r_1 of Fe_3O_4-contained liquid is much smaller than that of FeO-contained liquid and close to that of iron crystal. Hence, a smaller undercooling (75 °C) was obtained for Fe_3O_4-contained iron liquid.[23] Although the structural template effect of the substrate on liquid structure can not be directly observed in this experiment, it indicates that the atomic distance of the substrate does

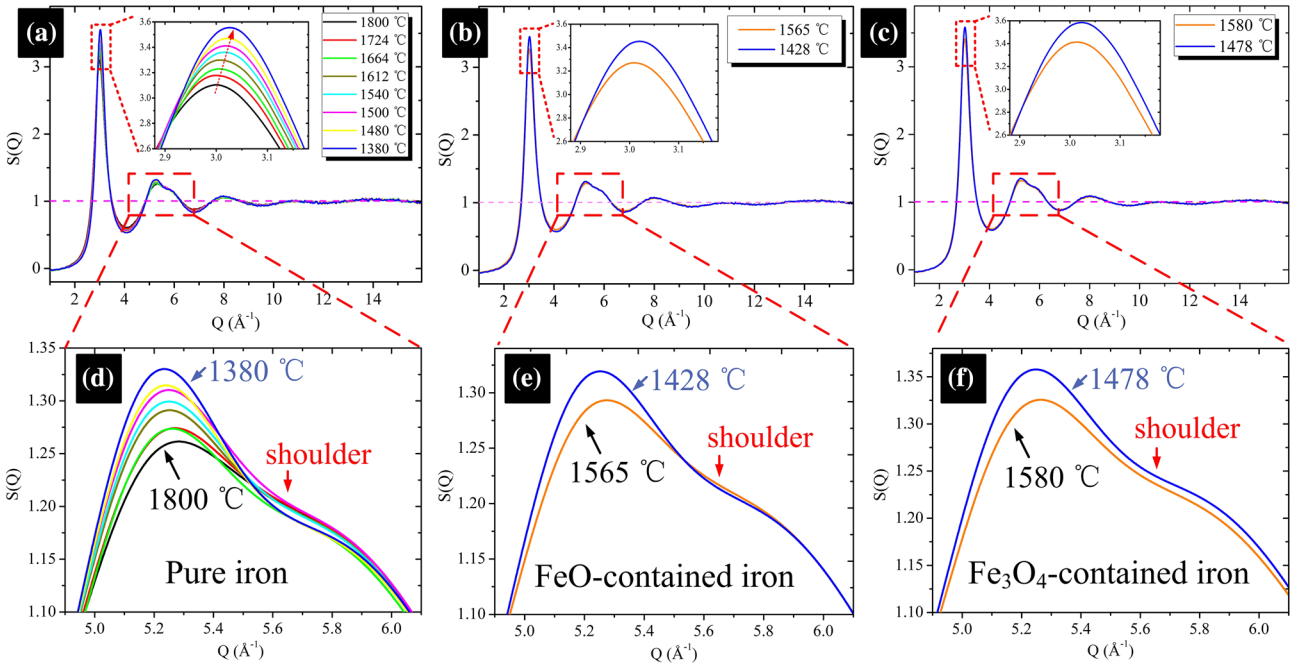

Fig. 1—Structure factors inferred from high-energy X-ray diffraction experiments and the enlarged second peaks of S(Q) marked in red squares for pure iron liquids (*a*, *d*), FeO-contained iron liquids (*b*, *e*), and Fe_3O_4-contained iron liquids (*c*, *f*) (Color figure online).

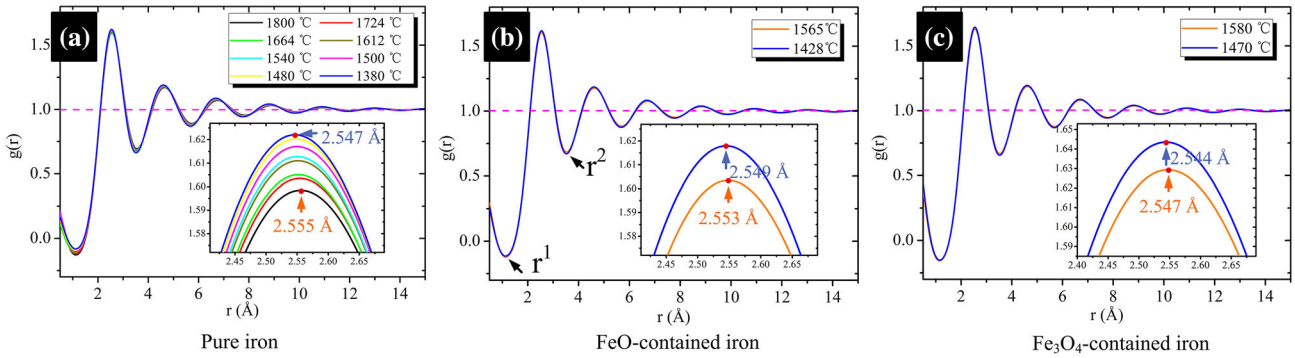

Fig. 2—The pair distribution functions g(r) for pure iron liquids (*a*), FeO-contained iron liquids (*b*), and Fe_3O_4-contained iron liquids (*c*).

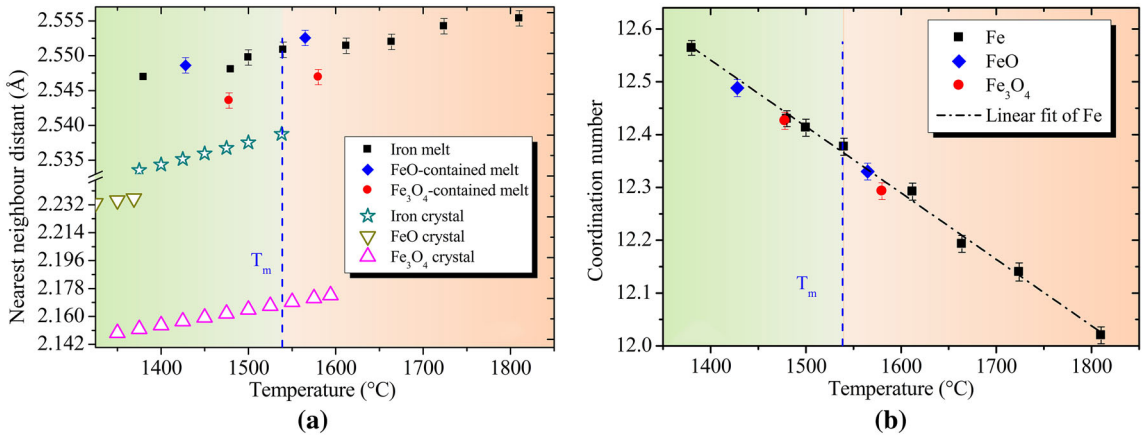

Fig. 3—(*a*) The nearest-neighbor distances, (*b*) coordination numbers of pure iron liquid (square symbol), FeO-contained iron liquid (diamond symbol), Fe_3O_4-contained iron liquid (circular symbol), iron crystal (star symbol), FeO crystal (down-triangle symbol), and Fe_3O_4 crystal (up-triangle symbol) change with temperature.

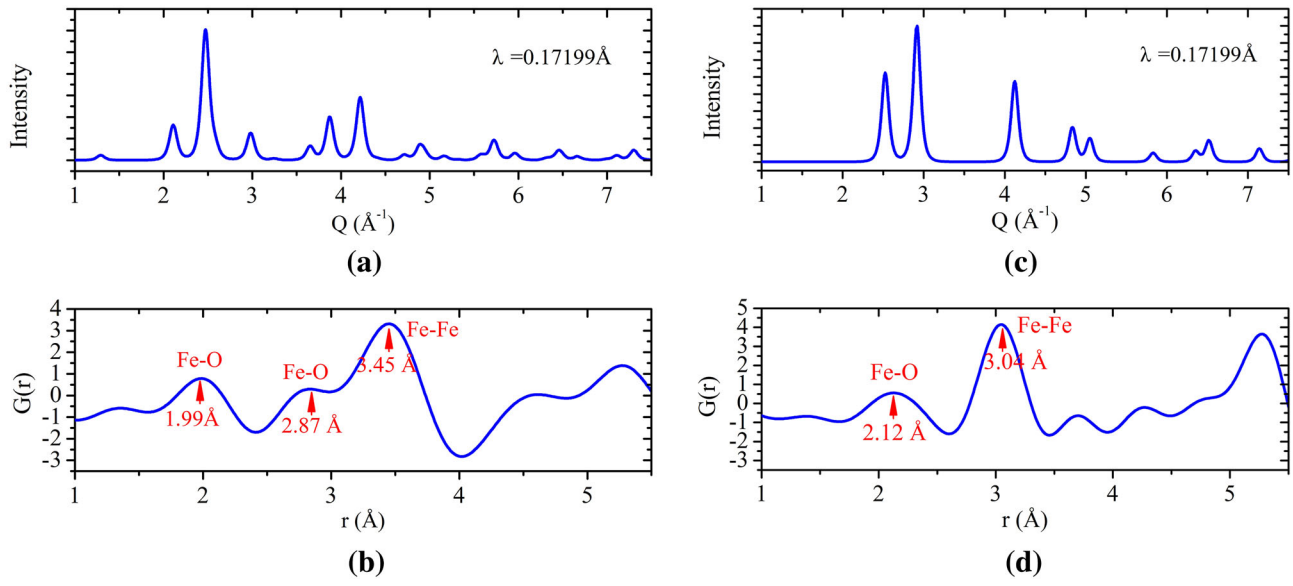

Fig. 4—(*a*) The X-ray diffraction intensity of Fe_3O_4 crystal as a function of Q and (*b*) the corresponding reduced pair distribution function G(r), (*c*) The XRD intensity of FeO crystal as a function of Q, and (*d*) the corresponding G(r).

affect the nucleation barrier of the liquid in terms of undercooling.

In summary, the liquid structure of pure iron was modified through the *in situ*-formed oxide particles. Synchrotron HE-XRD investigation indicates that a distinguished shoulder was observed at the high Q side of second peak of structure factors. It suggests that icosahedral-like orders should exist during the nucleation of the liquid investigated. The Z values of the liquids with and without oxides have the same trends with the decreasing temperature, but the r_1 reveals distinguished differences. The value of r_1 follows the sequence of r_1 (liquid iron) $\approx r_1$ (FeO-contained liquid) $> r_1$ (Fe_3O_4-contained liquid) $> r_1$ (solid iron) $> r_1$ (FeO crystal) $> r_1$(Fe_3O_4 crystal) at $T_{m,\ Fe}$ accompanying with the undercooling sequence of $\Delta T_{\text{pure liquid}}$ (304 °C) $> \Delta T_{\text{FeO-contained liquid iron}}$ (223 °C) $> \Delta T_{\text{Fe3O4-contained liquid iron}}$ (75 °C). It indicates that the liquid structural evolution during the cooling procedure can be manipulated by a proper substrate. A smaller atomic distance difference between the liquid and target crystal promises a decreased nucleation energy barrier for the new crystals in the liquid. The current study gives an unambiguous experimental proof of the atomic structural origin for the various undercoolings of the liquids cooled under a similar thermal condition and even containing similar liquid structure.

This study is supported by The National Key R&D Program of China (2017YFA0403802), the National Natural Science Foundation of China (51474148, 51727802, U1660203). The support of synchrotron high-energy X-ray diffraction by the BL13W1 beam line of Shanghai synchrotron radiation facility (SSRF), China, is gratefully acknowledged.

ELECTRONIC SUPPLEMENTARY MATERIAL

The online version of this article (https://doi.org/10.1007/s11661-018-4807-9) contains supplementary material, which is available to authorized users.

REFERENCES

1. D. Turnbull and B. Vonnegut: *Ind. Eng. Chem.*, 1952, vol. 44, pp. 1292–98.
2. M.E. Glicksman and W.J. Childs: *Acta Metallurgica*, 1962, vol. 10, pp. 925–33.
3. B.L. Bramfitt: *Metall. Mater. Trans. B*, 1970, vol. 1B, pp. 1987–95.
4. C. Sheng, J. Sun, D.P. Wang, Y.H. Zhang, L.J. Li, X.R. Chen, H.G. Zhong, and Q.J. Zhai: *J. Mater. Sci.*, 2018, vol. 53, pp. 4612–22.
5. D. Turnbull: *Proceedings of the international conference on physics of non-crystal solids*, 1965.
6. F. Spaepen and R.B. Meyer: *Scr. Metall.*, 1976, vol. 10, pp. 257–63.
7. F.C. Frank: *Proc. R. Soc. London, Ser. A*, 1952, vol. 215, pp. 43–46.
8. P. Ganesh and M. Widom: *Phys. Rev. B*, 2008, vol. 77, p. 014205.
9. M. Inui, K. Maruyama, Y. Kajihara, and M. Nakada: *Phys. Rev. B*, 2009, vol. 80, p. 180201.
10. M. Marques, L.E. Gonzalez, and D.J. Gonzalez: *Phys. Rev. B*, 2015, vol. 92, p. 134203.
11. G.W. Lee, A.K. Gangopadhyay, K.F. Kelton, R.W. Hyers, T.J. Rathz, J.R. Rogers, and D.S. Robinson: *Phys. Rev. Lett.*, 2004, vol. 93, p. 037802.
12. K.F. Kelton, G.W. Lee, A.K. Gangopadhyay, R.W. Hyers, T.J. Rathz, J.R. Rogers, M.B. Robinson, and D.S. Robinson: *Phys. Rev. Lett.*, 2003, vol. 90, p. 195504.
13. Y.T. Shen, T.H. Kim, A.K. Gangopadhyay, and K.F. Kelton: *Phys. Rev. Lett.*, 2009, vol. 102, p. 057801.
14. G. Kurtuldu, P. Jarry, and M. Rappaz: *Acta Mater.*, 2016, vol. 115, pp. 423–33.
15. J.M. How: *Philos. Mag. A*, 1996, vol. 74, pp. 761–75.
16. S.H. Oh, Y. Kauffmann, C. Scheu, W.D. Kaplan, and M. Ruhle: *Science*, 2005, vol. 310, pp. 661–63.
17. A. Hashibon, J. Adler, M.W. Finnis, and W.D. Kaplan: *Inerface Sci.*, 2001, vol. 9, pp. 175–81.
18. A. Hashibon, J. Adler, M.W. Finnis, and W.D. Kaplan: *Comp. Mater. Sci.*, 2002, vol. 24, pp. 443–52.
19. A.L. Greer: *Nat. Mater.*, 2006, vol. 5, pp. 13–14.
20. T.U. Schülli, R. Daudin, G. Renaud, A. Vaysset, O. Geaymond, and A. Pasturel: *Nature*, 2010, vol. 464, pp. 1174–77.
21. H. Reichert, O. Klein, H. Dosch, M. Denk, V. Honkimaki, T. Lippmann, and G. Reiter: *Nature*, 2000, vol. 408, pp. 839–41.
22. L. Wang, L. Yang, D. Zhang, M. Xia, Y. Wang, and J.G. Li: *Metall. Mater. Trans. A.*, 2016, vol. 47A, pp. 5012–22.
23. L. Wang, W. Lu, Q. Hu, M. Xia, Y. Wang, and J. Li: *Acta Mater.*, 2017, vol. 139, pp. 75–85.
24. K. Nakajima, H. Hasegawa, S. Khumkoa, and S. Mizoguchi: *Metall. Mater. Trans. B*, 2003, vol. 34B, pp. 539–47.
25. M. Xu, L. Wang, W. Lu, L. Zeng, H. Nadendla, Y. Wang, J. Li, Q. Hu, M. Xia, and J. Li: *Metall. Mater. Trans. A.*, 2018, vol. 49A, pp. 1762–69.
26. A.P. Hammersley: *J. Appl. Cryst.*, 2016, vol. 49, pp. 646–52.
27. N.A. Mauro, V. Wessels, J.C. Bendert, S. Klein, A.K. Gangopadhyay, M.J. Kramer, S.G. Hao, G.E. Rustan, A. Kreyssig, A.I. Goldman, and K.F. Kelton: *Phys. Rev. B*, 2011, vol. 83, p. 184109.
28. S. Sachdev and D.R. Nelson: *Phys. Rev. Lett.*, 1984, vol. 53, pp. 1947–50.
29. J. Ding, M. Xu, P.F. Guan, S.W. Deng, Y.Q. Cheng, and E. Ma: *J. Chem. Phys.*, 2014, vol. 140, p. 064501.
30. Y. Ishida, J. Wang, and T. Suga: *Acta Metall. et Mater.*, 1992, vol. 40, pp. S289–93.
31. M. Qian, P. Cao, M.A. Easton, S.D. Mcdonald, and D.H. Stjohn: *Acta Mater.*, 2010, vol. 58, pp. 3262–70.
32. D.H. Stjohn, M.A. Easton, M. Qian, and J.A. Taylor: *Metall. Mater. Trans. A.*, 2013, vol. 44A, pp. 2935–49.
33. Z. Chen, H. Kang, G. Fan, J. Li, Y. Lu, J. Jie, Y. Zhang, T. Li, X. Jian, and T. Wang: *Acta Mater.*, 2016, vol. 120, pp. 168–78.
34. M.M. Schneider and J.M. Howe: *Acta Mater.*, 2017, vol. 133, pp. 224–29.
35. E.M. Pouget, P.H.H. Bomans, J.A.C.M. Goos, P.M. Frederik, G. de With, and N.A.J.M. Sommerdijk: *Science*, 2009, vol. 323, pp. 1455–58.
36. S. Calvin, E.E. Carpenter, and V.G. Harris: *Phys. Rev. B*, 2003, vol. 68, p. 033411.
37. Y.F. Shen, J. Tang, Z.H. Nie, Y.D. Wang, Y. Ren, and L. Zuo: *Bioresour. Technol.*, 2009, vol. 100, pp. 4139–46.
38. T.J. Ahrens: *Mineral Physics and Crystallography: A Handbook of Physical Constants*, American Geophysical Union, Washington, DC, 1995.